JMEPEG (2012) 21:2701–2712
DOI: 10.1007/s11665-012-0264-6

1059-9495/$19.00

Reproducibility Study of NiTi Parts Made by Metal Injection Molding

M. Bram, M. Bitzer, H.P. Buchkremer, and D. Stöver

(Submitted March 26, 2012)

Powder metallurgy (P/M) is an attractive manufacturing process for net-shaped NiTi parts considering the limited machinability of NiTi alloys. Nevertheless, the industrial implementation of P/M processing for NiTi alloys is not trivial. To become competitive to manufacturing of NiTi alloys based on established ingot metallurgy, combination of fully pronounced shape memory behavior with sufficient mechanical properties is required. Successful use of P/M technology is strongly influenced by high affinity of NiTi alloys for uptake of oxygen and carbon, which leads to the formation of oxygen-containing Ti_2Ni and TiC phases coupled with increase of Ni content in the matrix. In the case of Ni-rich NiTi alloys, this increase leads to a shift of phase transformation temperatures to lower values. Furthermore, precipitation of Ni_4Ti_3 during cooling from sintering temperature is difficult to avoid. Even if these precipitates might be used to decrease the Ni:Ti ratio of the matrix balancing oxygen and carbon uptake, significant loss of ductility arises, especially in the case of finely dispersed Ni_4Ti_3 precipitates. In the present work, each step of P/M manufacturing is discussed regarding its influence on the specific properties of NiTi alloys. The work is based on the application of prealloyed, gas atomized NiTi powders. Metal injection molding was used for net-shaped manufacturing of tensile samples, which enabled detailed study of sintering behavior combined with investigation of shape memory and mechanical properties depending on particle size, oxygen and carbon content as well as precipitation of Ni_4Ti_3 phase.

Keywords intermetallics, nitinol, nonferrous metals, powder metallurgy, shape memory

1. Introduction

Powder metallurgy (P/M) techniques are promising for near-net-shaped manufacturing of NiTi alloys reducing tool wear and material loss to a minimum. Furthermore, constraints of ingot metallurgy like segregation and extensive grain growth can be avoided. Of the P/M techniques, it is metal injection molding (MIM) in particular, which is attractive for near-net-shaped production of NiTi components with complex geometries. This high-throughput process becomes economical particularly in the case of large-scale production.

For P/M processing of NiTi alloys, blends of Ni and Ti elemental powders as well as prealloyed NiTi powders can be used as starting materials. Since several decades, blends of Ni and Ti elemental powders are described in the literature for P/M manufacturing of NiTi alloys (Ref 1-6). Ductile behavior of elemental powders enables compaction by means of conventional pressing techniques. During thermal treatment, exothermic reaction between Ni and Ti leads to the formation of NiTi. Unfortunately, the main reaction is accompanied by the formation of significant amount of secondary phases like Ni_3Ti and Ti_2Ni (Ref 5-10), which embrittle the alloy and reduce the matrix volume contributing to the martensitic phase transformation. In the case of sufficient preheating, exothermic reaction becomes self-sustaining (denomination "combustion synthesis") and proceeds rapidly through the compact, while leaving large porosities in the range of 45-65 vol.% (Ref 1-6, 11). If thermal treatment is done with moderate heating rates, NiTi phase formation takes place by diffusion-controlled reaction sintering accompanied by the occurrence of Kirkendall porosity (Ref 7, 8, 10, 12-14). At temperatures above 942 °C, pore formation is supported by the occurence of partial eutectic melt (eutectic Ti-Ti_2Ni, Ref 15). In this case, typical porosities lie in the range of 30-40 vol.%. Even if porous NiTi is in clinical use for spine implants since several years (Ref 16, 17), high residual porosity, low mechanical strength, and residual amount of brittle secondary phases limited use of P/M NiTi for other applications so far.

If low porous, net-shaped NiTi parts with clearly improved shape memory behavior and mechanical properties are aspired, application of prealloyed NiTi powders is more promising. Even if this approach is already known from literature since the early 1980s (Ref 18-25), up to now less is published on net-shaped manufacturing of functional parts with fully pronounced shape memory effect or pseudoelasticity (Ref 26). Within the last decade, several comprehensive studies were conducted at our institute dealing with the P/M production of NiTi parts starting from prealloyed NiTi powders and using the MIM process for net-shaped manufacturing (Ref 12, 27-33). From industrial point of view, this process has big potential for high-throughput and high-precision production of complex-shaped NiTi parts in large quantities. MIM transfers extensive

This article is an invited paper selected from presentations at the International Conference on Shape Memory and Superelastic Technologies 2011, held November 6-9, 2011, in Hong Kong, China, and has been expanded from the original presentation.

M. Bram, M. Bitzer, H.P. Buchkremer, and **D. Stöver,** Forschungszentrum Jülich GmbH, Institute of Energy and Climate Research (IEK-1: Materials Synthesis and Processing), 52425 Jülich, Germany. Contact e-mail: m.bram@fz-juelich.de.

capability of thermo-plastic shaping to P/M parts. Within the last years, we demonstrated the potential of MIM for net-shaped manufacturing of NiTi parts in several case studies including tensile sample, biomedical foot staple, and pipe connector sleeve (Ref 27, 29, 30, 32). Furthermore, net-shaped parts with functional macro pores were produced recently using suitable space holder materials (Ref 34-36). Based on the comprehensive experience achieved in these studies, it becomes possible to draw a number of general conclusions on the main factors influencing the specific properties of net-shaped NiTi parts made by P/M technologies. In the present work, a detailed discussion of each factor is given. Furthermore, boundary conditions are discussed, which must be fulfilled to improve reproducibility of P/M technologies starting from prealloyed NiTi powders.

2. Experimental

In the present work, only prealloyed NiTi powders were used as starting materials. Up to now, availability of such powders on an industrial scale is still limited. Therefore, all NiTi powder batches applied in this study were produced by gas atomization starting from commercial NiTi rods. The rods had nominal Ni-contents in the range of 49.5-50.85 at.%. Usually, Ni content of these NiTi rods is calculated from M_s temperature using well-known curves of Tang et al. (Ref 37), Khalil-Allafi et al. (Ref 38), or Frenzel et al. (Ref 39). Two methods were considered for gas atomization of the rods. In the Nanoval process (Nanoval GmbH, Berlin, Germany), the rods were melted in graphite crucible and gas atomized by a Laval nozzle using argon gas with supersonic velocity (Ref 40). Main advantage of this process is high amount of small particles suitable for MIM processing. Approximately 90% of powder particles were smaller than 45 µm. Disadvantages are distinct number of inaccurate powder particles like hollow spheres or satellites (small particles adhere on the surface of larger ones, Fig. 1a), increased oxygen contents resulting from the atomization process, increased carbon contents caused by the contact of the NiTi melt with crucible as well as limited reproducibility of powder batches even when produced with the same parameter set (Table 1). Alternatively, NiTi powders were produced by TLS Technik GmbH & Co Spezialpulver KG (Bitterfeld, Germany) using electrode induction inert gas atomization (EIGA) of NiTi rods, where atomization of the melt heated by induction was done by highly pressurized argon (purity 99.9999 vol.%, oxygen below 0.5 ppm) without contact to graphite crucible or ceramic nozzle (Ref 41). Powder morphology is characterized by clearly reduced amount of satellites and hollow spheres (Fig. 1b) as well as reduced oxygen and carbon contents. Unfortunately, amount of particles <45 µm is $<30\%$, making the EIGA process less attractive for MIM applications on an industrial scale. After gas atomization, the powder batches were fractionized by the manufacturers to small (<25 µm), intermediate (25-45 µm), and coarse sized (45-100 µm) powder fractions, which were used for MIM processing and hot isostatic pressing (HIP) as a reference. Fractionizing was done by sieving. Particle fractions larger than 100 µm were not considered in this study.

Table 1 summarizes the impurity contents and particle size distributions of all powder fractions used in this work. In the case of powders made by the Nanoval process, oxygen and carbon varied between 0.05-0.18 wt.% and 0.03-0.10 wt.%. Not unexpected, impurity contents are significantly higher in the case of smaller powder fractions. Nevertheless, even in the case of fractions with similar particle size distribution, scattering of impurity contents between nominal identical powder batches indicates the need of optimized processing parameters for improved reproducibility. Contrary, NiTi powders produced by EIGA process are characterized by lower impurity contents (oxygen 0.04-0.10 wt.%, carbon 0.01-0.03 wt.%) coupled with improved reproducibility and powder quality. Again, increased oxygen contents were found in the case of smaller powder fractions (TLS05, TLS06). These powder fractions are currently in use for manufacturing dental brackets by µ-MIM technology.

For compensating of increased Ni:Ti ratio in the case of oxygen and carbon uptake during P/M processing, powder fraction TLS04 was blended with 1 at.% of Ti powder, which was produced by EIGA (TLS GmbH, Bitterfeld, Germany) as well. Particle size distribution of this powder was d_{10} = 12 µm, d_{50} = 34 µm, and d_{90} = 63 µm.

In this work, we abdicated to measure phase transformation temperatures of starting powder fractions. Considering their rapid solidification after gas atomization, NiTi powders are far from thermodynamic equilibrium. Therefore, Ni:Ti ratio of individual powder particles depends on their solidification rate,

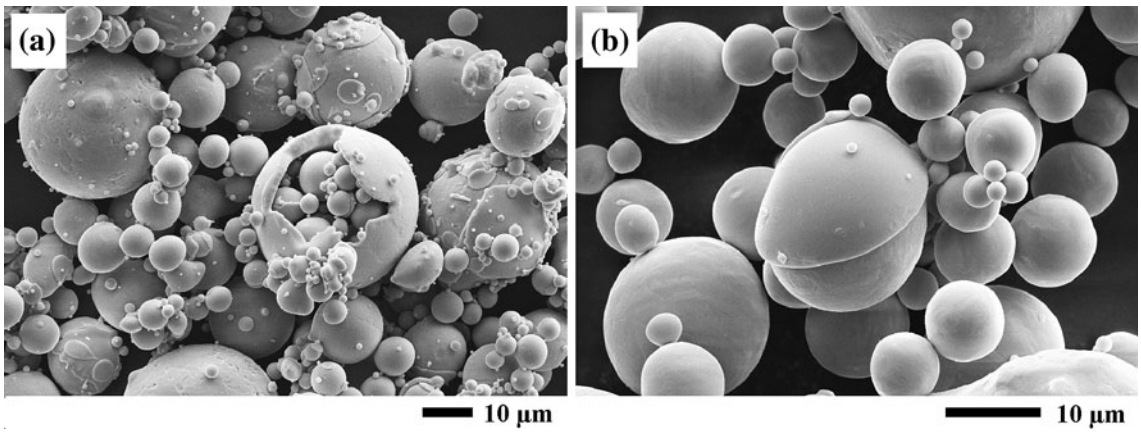

Fig. 1 Morphology of prealloyed NiTi powders prepared by gas atomization. (a) Nanoval process (Ref 40) and (b) EIGA (Ref 41)

Table 1 Powder fractions considered in this work, manufactured by gas atomization using the Nanoval process (Nanoval, Berlin, Germany) as well as the EIGA process (TLS GmbH, Bitterfeld, Germany)

Powder fraction	Batch name	Particle size, µm			Impurity content, wt.%			Ni content, at.%
		d_{10}	d_{50}	d_{90}	O	C	N	
Nan01	K173F	7	18	51	0.05	0.07	0.002	50.85 (Ref 28)
Nan02	N38Z	4	10	25	0.09	0.03	0.003	50.85 (Ref 28)
Nan03	H128B	8	18	37	0.14	0.08	0.004	50.85 (Ref 28)
Nan04	N37B	9	21	45	0.06	0.07	0.002	50.85 (Ref 28, 42)
Nan05	H189B	8	20	59	0.10	0.08	0.002	49.5 (Ref 28)
Nan06	H189Z	3	8	21	0.18	0.10	0.002	49.5 (Ref 28)
TLS01	0449/3	46	67	108	0.04	0.02	<0.01	50.6 (Ref 30, 32)
TLS02	0449/3	8	22	41	0.04	0.03	<0.01	50.6 (Ref 30, 32)
TLS03	Unlabeled	7	21	40	0.06	0.03	<0.01	49.7 (Ref 33)
TLS04	1026/3	6	11	20	0.05	0.03	<0.001	50.8
TLS05	1264/3	8	14	23	0.10	0.01	n.m.	50.8
TLS06	1394/3	8	13	20	0.09	0.02	n.m.	50.8

n.m., Not measured

particle size, and impurity content leading to broad ranges of phase transformation temperatures within each powder fraction. Mentz et al. (Ref 33) investigated the phase transformation temperatures of substoichiometric NiTi powder depending on particle size. With increasing particle size, transfer from single-step to multiple-step phase transformation was found. Similar results were also reported by Bansiddhi and Dunand (Ref 42). Nevertheless, scattering of phase transformation temperatures of gas atomized powder particles might be of less importance for evaluating the reproducibility of P/M NiTi, since subsequent consolidation by diffusion processes at temperatures above 1050 °C (HIP) or above 1200 °C (pressureless sintering) is equivalent to homogenization treatment usually applied for NiTi parts made by ingot metallurgy (Ref 39). In the case of P/M, it must be considered that during furnace cooling from sintering temperature, the temperature range of 630-350 °C is passed through slowly if using conventional sintering equipment. As a consequence, precipitation of meta-stable Ni_4Ti_3 phase is unavoidable (Ref 43). Since cooling rates strongly depend on size and loading of furnace as well as sample dimension, it is almost impossible to achieve controlled precipitation states already after sintering. Therefore, solution treatment with subsequent annealing at well-defined temperatures is mandatory for achieving reproducible properties. Characteristic cooling rates of sintering equipment used in this work are given below.

For investigation of Ni_4Ti_3 precipitation depending on annealing temperature, NiTi samples were prepared by HIP using powder fraction Nan04. For load transfer, the powder was filled in steel capsules (material 1.4571). Afterward, capsules were evacuated and gas tight welded. HIP was conducted for 3 h at 1065 °C and 100 MPa. In the temperature range of 630-350 °C, the cooling rate of HIP device (EPSI, Temse, Belgium) was 5 K/min, which was the maximum rate accessible with this device. Therefore, it took approximately 1 h to pass through the temperature range capable for Ni_4Ti_3 precipitation. After HIP, capsules were removed by mechanical machining. Then, NiTi alloy was solution treated at 1000 °C for 1 h followed by water quenching. Afterward, thermal treatments were conducted in the temperature range between 430 and 630 °C using dwell times of 1 h in each case. Again, samples were water quenched after annealing.

For MIM processing, feedstocks were prepared by mixing NiTi powders with two component binder system consisting of paraffin and polyethylene mixed in a ratio of 60:40 (in vol.%). The solid content of feedstocks was consistently 64 vol.%. Arburg MD270-440/140 injection molding machine was used for manufacturing of tensile samples. Detailed description of sample geometry, MIM process parameters, and debinding conditions can be found elsewhere (Ref 29).

A comprehensive sintering study was carried out on prealloyed NiTi powders made by Nanoval process. The study was done on samples produced by MIM and aimed on understanding the influence of particle size, impurity content, and Ni-content on the sintering behavior. After debinding, samples were placed on Y_2O_3 sintering aid. Sintering was conducted using a vacuum furnace (Thermal Technology, 121212 WM, Santa Rosa, CA, USA), varying the temperature to 1150, 1200, 1230, 1250, 1265, and 1270 °C. Sintering was consistently done in vacuum ($p < 10^{-3}$ Pa). In each case, the dwell time was 5 h with heating and cooling rates of 5 K/min. Considering this cooling rate, it took again approximately 1 h to pass through the critical temperature range of 630-350 °C. Therefore, Ni_4Ti_3 precipitation state was expected to be comparable to HIP samples. Technically, increased cooling rates up to 10 K/min were possible, but uncontrolled precipitation of Ni_4Ti_3 is still expected. Therefore, related attempts were omitted. Sintering temperatures higher than 1270 °C were restricted due to approaching the melting temperature of NiTi (T_m = 1310 °C, Ref 15) increasing the risk of chemical interaction with the sintering aid.

Phase transformation temperatures were characterized by DSC measurements (TA Instruments, 2920 MDSC) with heating and cooling rates of 10 K/min in the temperature range of −100 °C and +150 °C. Microstructures were characterized with a SEM (LEO 1530 VP) equipped with an energy dispersive microanalysis (EDX) unit. Chemical analysis was performed to investigate the impurity contents. Oxygen and nitrogen contents were analyzed by the inert gas fusion infrared method and carbon by the combustion infrared absorption method. Tensile tests up to fracture were conducted on a Zwick/Roell Z100 device with a crosshead speed of 0.5 mm/min. The elongation was measured by an extensometer. All tensile tests were done under temperature control in a climate chamber.

3. Results and Discussion

3.1 Sintering Behavior of Prealloyed NiTi Powders

Prealloyed NiTi powders require sintering temperatures approaching the melting point of NiTi (T_m = 1310 °C, Ref 15) to achieve densities higher than 90% of theoretical density (ρ (NiTi) = 6.45 g/cm^3). Low sintering activity of prealloyed NiTi powders is caused by high degree of order of intermetallic NiTi lattice coupled with high activation energies for diffusion processes (Ref 44, 45). Even if sintering densities are influenced by inaccurate powder particles like hollow spheres or satellites, some significant trends are obvious.

3.1.1 Influence of Particle Size. As expected, fine powder fractions lead to the highest sintering densities. The maximum sintering density lied in the range of 96-97% of theoretical density and was achieved already after 5 h at 1230 °C with Ni-rich powder Nan02 (d_{10} = 4 µm, d_{50} = 10 µm, d_{90} = 25 µm) for 5 h (Fig. 2a). In this case, higher sintering temperatures or longer dwell times did not improve the maximum sintering density further. In the case of Ni-rich powder Nan01 with intermediate particle size (d_{10} = 7 µm, d_{50} = 18 µm, d_{90} = 51 µm), sintering density was significantly lower with 92% at 1230 °C and 94% at 1250 °C, both for 5 h (Fig. 2b). The same trend was found for substoichiometric NiTi powders.

3.1.2 Influence of Ni-Content. At given sintering conditions and comparable particle sizes, Ni-rich NiTi alloys tend to show significantly enhanced sintering densities (e.g., Nan02 vs. Nan06, Fig. 2a). With increasing particle size, this effect becomes more pronounced (Nan01 vs. Nan05, Fig. 2b). It is supposed that this effect is related to lower activation energy for diffusion of Ni atoms compared to diffusion of Ti atoms. The higher mobility of Ni atoms is probably caused by smaller atom radius of Ni (radius (Ni) = 0.1244 nm, radius (Ti) = 0.1448 nm, Ref 46). A similar effect is discussed in literature as main reason for formation of Kirkendall porosity in the case of sintering elemental Ni and Ti powder blends (Ref 8).

For substoichiometric NiTi alloys with intermediate particle size, it was not possible to achieve sintering densities higher than 90%. For powder fraction Nan05, sintering density was only 83% at 1250 °C, 5 h and increased to 90% at 1265 °C, 5 h. Alternatively, the same sintering density was achieved for this powder if dwell time at 1250 °C was increased to 10 h. However, doubling of dwell time to 20 h did not change the sintering density further.

3.1.3 Influence of Improved Powder Quality. Reducing the amount of hollow spheres and satellites using powders produced by the EIGA process was another attempt for improving the sintering density. Here, optimized sintering conditions achieved with Nanoval powders (1250 °C, 5 h) were transferred to EIGA powders TLS02 and TLS03. Even with improved powder quality, same trends were obvious. As shown in Fig. 2(b), Ni-rich TLS02 powder (50.6 at.% Ni) had a higher sintering density of 90% than substoichiometric TLS03 powder (49.7 at.% Ni). In the latter case, sintering density was only 85% (Ref 32, 33). The result also indicates that reduced oxygen and carbon contents did not change the sintering activity significantly.

3.2 Formation of Oxygen-Containing Ti_2Ni and TiC Phases

While uptake of nitrogen can be almost neglected during P/M processing of NiTi alloys, uptake of oxygen and carbon is unavoidable. In addition to impurity contents already picked up during gas atomization, further increase is caused by contact of NiTi powders with organic binder in the case of MIM processing and residual oxygen from protective atmosphere during sintering. Table 2 compares impurity contents of starting powders with P/M parts made by MIM and HIP.

As expected, there is almost no change of impurity contents after HIP due to encapsulation in evacuated steel capsules. In the case of MIM processing, the use of paraffin-polyethylene-based binder system enabled to keep the carbon uptake below 0.01 wt.%, resulting in total carbon content of MIM parts of 0.08-0.10 wt.% in the case of Nanoval powders and 0.03-0.04 wt.% in the case of EIGA powders. Oxygen uptake was significantly higher and lied in the range of 0.05-0.09 wt.%. After sintering, oxygen content of NiTi parts manufactured by MIM was up to 0.23 wt.% in the case of Nanoval powders and typically varied between 0.12 and 0.17 wt.% in the case of EIGA powders. By trend, decreasing particle size is coupled with higher oxygen uptake.

Contrary to established titanium alloys, where oxygen and carbon are almost completely solved in the Ti lattice on interstitial sites (Ref 48, 49), there is almost no solubility of oxygen (<0.0045 at.%) and carbon in the NiTi matrix (Ref 50-53). Therefore, formation of oxygen-containing

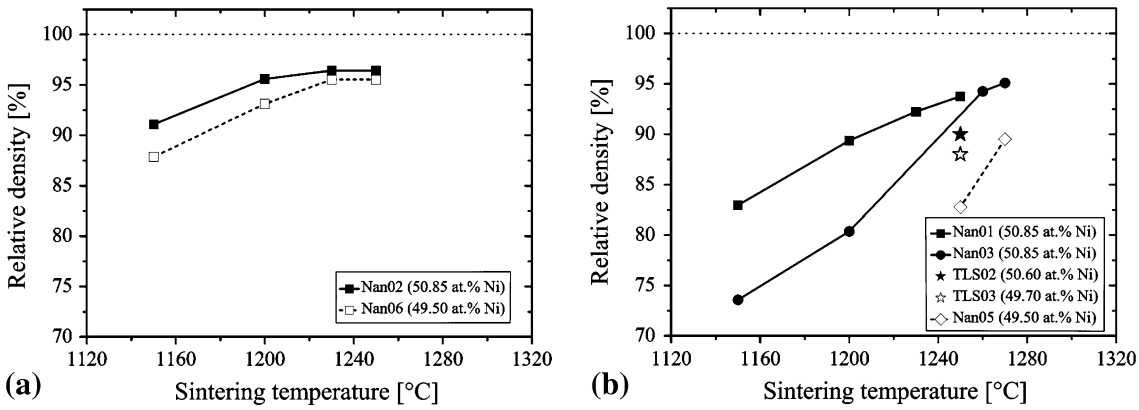

Fig. 2 Sintering study of MIM parts depending on powder size fraction and sintering temperature at constant dwell time of 5 h, relative density in percentage of theoretical density (6.45 g/cm^3). (a) Small particle size fractions <25 µm (Ref 28) and (b) intermediate particle size fractions 25-45 µm (Ref 28, 32, 33)

Table 2 Uptake of oxygen (O), carbon (C), and nitrogen (N) after HIP and MIM

	O, Gew. %	C, Gew. %	N, Gew. %	References
Powder Nan04	0.06	0.07	0.002	31
HIP sample (Nan04, 1065 °C, 100 MPa, 3 h)	0.07	0.07	0.001	
Powder Nan06	0.18	0.10	0.002	29
MIM part (bone staple) after sintering (Nan06, 1230 °C, 5 h, vacuum)	0.23	0.08	0.004	
Powder TLS01	0.04	0.02	0.002	30, 32
HIP sample (TLS01, 1050 °C, 100 MPa, 3 h)	0.04	0.03	0.002	
Powder TLS02	0.05	0.03	0.002	30, 32
MIM tensile sample after sintering (TLS02, 1250 °C, 10 h, Vacuum)	0.12	0.03	0.004	
Powder TLS02	0.05	0.03	0.002	47
MIM part (porous cylinder) (TLS02, 1250 °C, 10 h, Vacuum)	0.14	0.04	0.002	

Ti_2Ni (in literature often named "Ti_4Ni_2O" or "$Ti_4Ni_2O_x$" with $0 \leq x \leq 1$, Ref 44, 53-55) as well as TiC phases result. Oxygen was found to stabilize the Ti_2Ni phase also in the case of Ni-rich NiTi alloys (Ref 39). Furthermore, these secondary phases preferentially remove Ti from the NiTi matrix, which is coupled with increasing the Ni:Ti ratio and lowering the phase transformation temperatures following the relationship given by Tang et al. (Ref 37), Khalil-Allafi et al. (Ref 38), or Frenzel et al. (Ref 39). The negligible solubility of oxygen and carbon in the NiTi lattice might explain why there is obviously no influence of impurity contents on sintering behavior. Main mechanism of densification during sintering of prealloyed NiTi powders is volume diffusion of Ni and Ti atoms in the NiTi grains. Considering that almost no interstitial atoms can be solved in NiTi lattice, which might influence volume diffusion of Ni and Ti atoms, diffusion coefficients remain almost constant even in the case of oxygen and carbon uptake.

Figure 3 compares the distribution of oxygen-containing Ti_2Ni and TiC phases of starting powder fraction Nan04, after HIP (conducted with Nan04 at 1065 °C, 100 MPa, 3 h) and after MIM processing (sintering of Nan06 at 1250 °C, 5 h). Obviously, secondary phases can already be found finely distributed in the starting powder (Fig. 3a). Microstructural investigations by WDX (not shown here) indicate light gray phase as oxygen-containing Ti_2Ni, while TiC precipitates appear as dark gray phase. After thermal treatment, secondary phases were preferentially located on the surface of formerly powder particles, as shown in Fig. 3(b). With increasing sintering temperature, coarsening of both phases took place, which is more pronounced in the case of oxygen-containing Ti_2Ni phase (Fig. 3b, d). This result is in contrast to literature, where it is stated that size of these phases is not affected by thermal treatments even at temperatures up to 1200 °C (Ref 53). Additionally, residual porosity can be clearly seen in Fig. 3(c, d) for pressureless sintered MIM samples as expected from sintering studies discussed before. Oxygen-containing Ti_2Ni phase as well as pores were identified to be the main origin of fracture in tensile tests (Fig. 4). A detailed discussion can be found elsewhere (Ref 30, 32).

3.3 Precipitation of Meta-stable Ni_4Ti_3

It is well known from the literature that precipitation of meta-stable Ni_4Ti_3 phase might occur in the temperature range between 350 and 630 °C if Ni-content exceeds 50 at.% (Ref 43). This effect must be carefully taken into account for P/M manufacturing of NiTi alloys since this temperature range is passed through slowly during furnace cooling from sintering temperature resulting in uncontrolled precipitation states. Examples of dwell times in the critical temperature range are given in Chapter 2 for conventional HIP device and vacuum furnace. Therefore, for the adjustment of reproducible mechanical and shape memory properties it becomes necessary to conduct solution treatment after sintering followed by water quenching. Afterward, well-defined precipitation of Ni_4Ti_3 can be optionally achieved by thermal treatment in the abovementioned temperature range. As an example, Fig. 5 shows size of Ni_4Ti_3 precipitates in NiTi sample made by MIM after annealing at 500 and 550 °C, each for 1 h (Ref 28). In general, controlled precipitation of Ni_4Ti_3 can be used to adjust phase transformation temperatures including R-phase transformation if required for application (Ref 56).

A detailed study on influence of Ni_4Ti_3 precipitations on phase transformation was conducted on hot isostatically pressed samples made of powder Nan04. Figure 6 summarizes the main results (Ref 31). In the as-HIPed state (Fig. 6a), phase transformation was characterized by broad peaks indicating inhomogeneous precipitation state coupled with superposition of transformation peaks including R-phase transformation. The weakly pronounced peak during cooling is probably related to this R-phase, while the martensite peak is assumed to be outside the measurement range.

After solution treatment at 1000 °C, 1 h with subsequent water quenching, complete solution of Ni_4Ti_3 phases was assumed. DSC measurements after solution treatment indicated that the martensite transformation peak lies below −100 °C (Fig. 6b). Consequently, increased Ni-content of NiTi matrix phase was supposed after HIP. Considering the curve of Tang et al. (Ref 37), Ni content of 50.85 at.% in starting material was increased to value slightly higher than 51.1 at.%. This shift is caused by change of Ni:Ti ratio in the matrix due to formation of oxygen-containing Ti_2Ni and TiC phases as discussed before. In the present case, main uptake of oxygen and carbon took place during powder production.

Investigation of phase transformation temperatures after annealing in a temperature range between 430 and 540 °C (Fig. 6c to e) clearly indicated the formation of the R-phase. With increasing annealing temperature, the transition temperature of the R-phase formation during cooling was reduced (peak temperatures 23, 21, and −2 °C) which is attributed to the increasing size of the Ni_4Ti_3 precipitations. Vice versa, the peak temperature of the martensite transformation was increased (below −100, −70, and −40 °C). It is supposed that stresses around the coherent and semi-coherent Ni_4Ti_3 precipitations are the main reason for this effect. A more detailed discussion on influence of Ni_4Ti_3 precipitations on martensitic

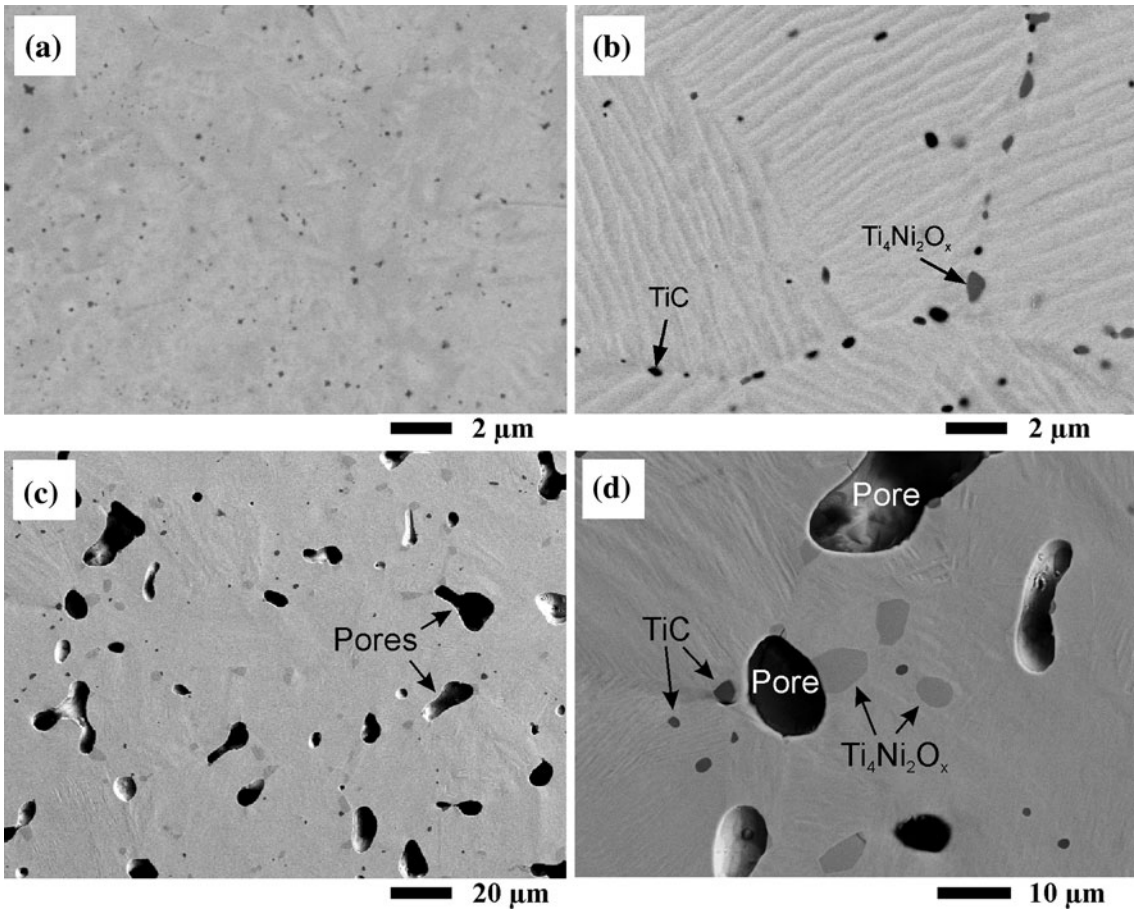

Fig. 3 Investigation of microstructures. (a) Powder particle (Nan04), (b) distribution of secondary phases after HIP (Nan04, 1065 °C, 100 MPa, 3 h) (Ref 31), (c) microstructure of NiTi sample made by MIM (TLS02, 1250 °C, 5 h, residual porosity 10%), and (d) detail of (c)

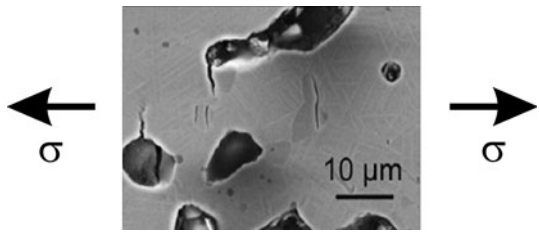

Fig. 4 Oxygen-containing Ti_2Ni phase and pores as the main origin of fracture in tensile tests (Ref 28)

phase transformation can be found in the literature (Ref 43, 56-58). With further increase of annealing temperature, both peaks approached each other. After annealing at 580 °C (Fig. 6f), R-phase peak disappeared, while the martensite peak temperature was reduced to −56 °C. This trend continued after annealing at 630 °C (Fig. 6g). Here, it is supposed that the martensite peak felt outside the measurement range again. In this case, precipitations are assumed to become completely incoherent to the matrix and thus, their influence on phase transformation becomes negligible.

Also in the case of the austenite peaks, significant differences exist between material after solution treatment and after controlled annealing in the temperature range 430-630 °C. After solution treatment (Fig. 6b), low austenite peak temperature (−67 °C) was found. After annealing at 430 °C (Fig. 6c), two-step phase transformation back to austenite with peak temperatures of 6 and 37 °C occured. Further, shift of peak temperatures to 19 and 32 °C was found after annealing at 480 °C (Fig. 6d) resulting in a single peak at 22 °C after annealing at 540 °C (Fig. 6e). In the case of annealing at 580 °C, initially decrease of peak temperature to −4 °C was observed again (Fig. 6f). Finally, after annealing at 630 °C (Fig. 6g), austenite peak disappeared, probably due to an incomplete phase transformation into martensite. Comparing the different graphs after heat treatment, annealing at 430 °C (Fig. 6b) approaches the phase transformation behavior of samples in the as HIPed state in the best way. Therefore, it is supposed that in the case of furnace cooling of P/M NiTi alloys with a cooling rate of 5 K/min, a precipitation state of Ni_4Ti_3 occurs, which is quite similar to the precipitation state after annealing in a temperature range of 400-450 °C.

3.4 Mechanical Properties of MIM Samples

To investigate the upper limit of mechanical properties obtainable with P/M technologies, tensile tests were conducted on tensile samples produced by HIP (Ref 30, 32). Using powder fraction TLS03 as starting material, fracture strains up to 16% in the austenitic and 20% in the martensitic state were achieved after solution treatment. The fracture stress was approximately 800 MPa. SEM investigation of fracture surface indicated intergranular fracture. Controlled coarsening of oxygen-containing Ti_2Ni phase by additional high-temperature

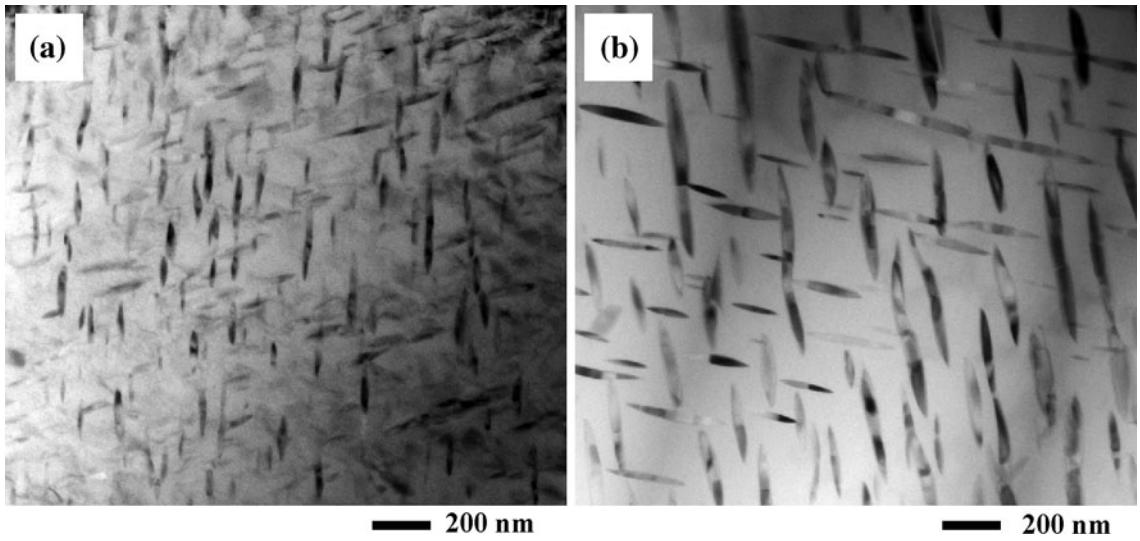

Fig. 5 TEM investigation of NiTi sample made by MIM starting from powder fraction Nan01 (sintered at 1250 °C, 5 h, solution treated at 1000 °C, 1 h, subsequent water quenching). Thermal treatment at (a) 500 °C and (b) 550 °C, 1 h (Ref 28)

treatment at 1250 °C, 10 h in vacuum led to increase of fracture strain up to 22% in the austenitic and 33% in the martensitic state (solution treated), while fracture stress stayed almost constant in the range of 800-850 MPa. Change from intergranular to transgranular fracture was found, which is discussed more detailed elsewhere (Ref 30, 32).

If tensile samples were prepared by MIM, martensitic stress plateau and mechanical properties are influenced by three factors (I) residual porosity (II) oxygen-containing Ti_2Ni and TiC phases, and (III) Ni_4Ti_3 precipitates. Due to further up-take of oxygen and carbon during each step of MIM processing and higher sintering temperatures, volume content and size of secondary phases were even larger than in the as-HIPed case. As already shown in Fig. 4, cracks are mainly originated from the oxygen-containing Ti_2Ni phases under tensile load. Crack propagation becomes easier in MIM due to the higher amount of these secondary phases. On the other hand, residual microporosity in the range of 3-12 vol.% resulted from the pressureless sintering process is another source of reduced stiffness, fracture stress, and fracture strain. Considering Fig. 2, residual microporosity increases with increasing particle size and decreasing Ni-amount.

For tensile samples produced by MIM, fracture stress lied in the range of 400-750 MPa, which is significantly lower than for samples made by HIP or ingot metallurgy. Obviously, this result is mainly caused by residual microporosity. Figure 7(a) emphasizes the risk of testing P/M NiTi samples in the furnace cooled condition omitting solution treatment. Fracture strains in the range of 6-7% resulted in this case, independent of the fact that residual microporosity was only 3%. Nevertheless, even for these samples it was possible to conduct more than 50 pseudoelastic cycles up to 2% strain without failure in the fully austenitic state (Fig. 7b).

It is well known from NiTi alloys prepared by ingot metallurgy that finely dispersed and small-scaled Ni_4Ti_3 precipitations have highest impact on mechanical properties. Miyazaki et al. (Ref 59) showed in their study that tensile samples with 50.5 and 50.9 at.% Ni annealed in the temperature range of 300-500 °C showed increased yield strengths in combination with clearly reduced fracture strains. Considering these results, uncontrolled precipitation of Ni_4Ti_3 during furnace cooling from sintering temperature should be strictly avoided in the case of P/M manufacturing of NiTi alloys.

After conducting solution treatment, clearly improved fracture strains up to 17% in the austenitic and up to 20% in the martensitic state were found for substoichiometric NiTi alloys after solution treatment (950 °C, 1 h), even if residual porosity approaches 12 vol.% (Fig. 7c) (Ref 60). For Ni-rich alloys, residual porosities of MIM tensile samples lied in the range of 3-10 vol.% (Fig. 3c), mainly depending on the particle size of the starting powders. Unexpected, fracture strains were even lower with 9% in the austenitic and 16% in the martensitic state after solution treatment (Fig. 7d). Controlled precipitation of finely dispersed Ni_4Ti_3 by thermal treatment at 450 °C for 1 h led to further decrease of ductility characterized by significant loss of fracture strain to 6% in the austenitic and 9% in the martensitic state, which is in accordance with the work of Miyazaki et al. (Ref 59) on NiTi made by ingot metallurgy.

3.5 Martensitic Stress Plateau

All P/M NiTi samples, which were tested under tensile conditions, showed clearly pronounced martensitic stress-plateaus. As expected, the plateau stress rose with increasing testing temperatures due to the increased stability of the austenitic phase at higher temperatures (Fig. 7a). In general, the length of the plateau was in the range of 4-5% (Ref 29, 30, 32, 60), which is lower than usually reported for NiTi alloys manufactured by ingot metallurgy (Ref 59, 61-64). Furthermore, the plateau was always characterized by continuous increase of stress with increasing strain. It is supposed that in the case of P/M NiTi, isotropic orientation of the NiTi grains in combination with enhanced amount of oxygen-containing Ti_2Ni and TiC phases are the main reasons for this behavior. Lattice mismatch on grain boundaries, these secondary phases as well as stress fields around them hinder proceeding of martensitic accommodation processes while supporting formation of dislocations. Furthermore, precipitation of meta-stable Ni_3Ti_4 increases the slope of the martensitic plateau (Ref 32,

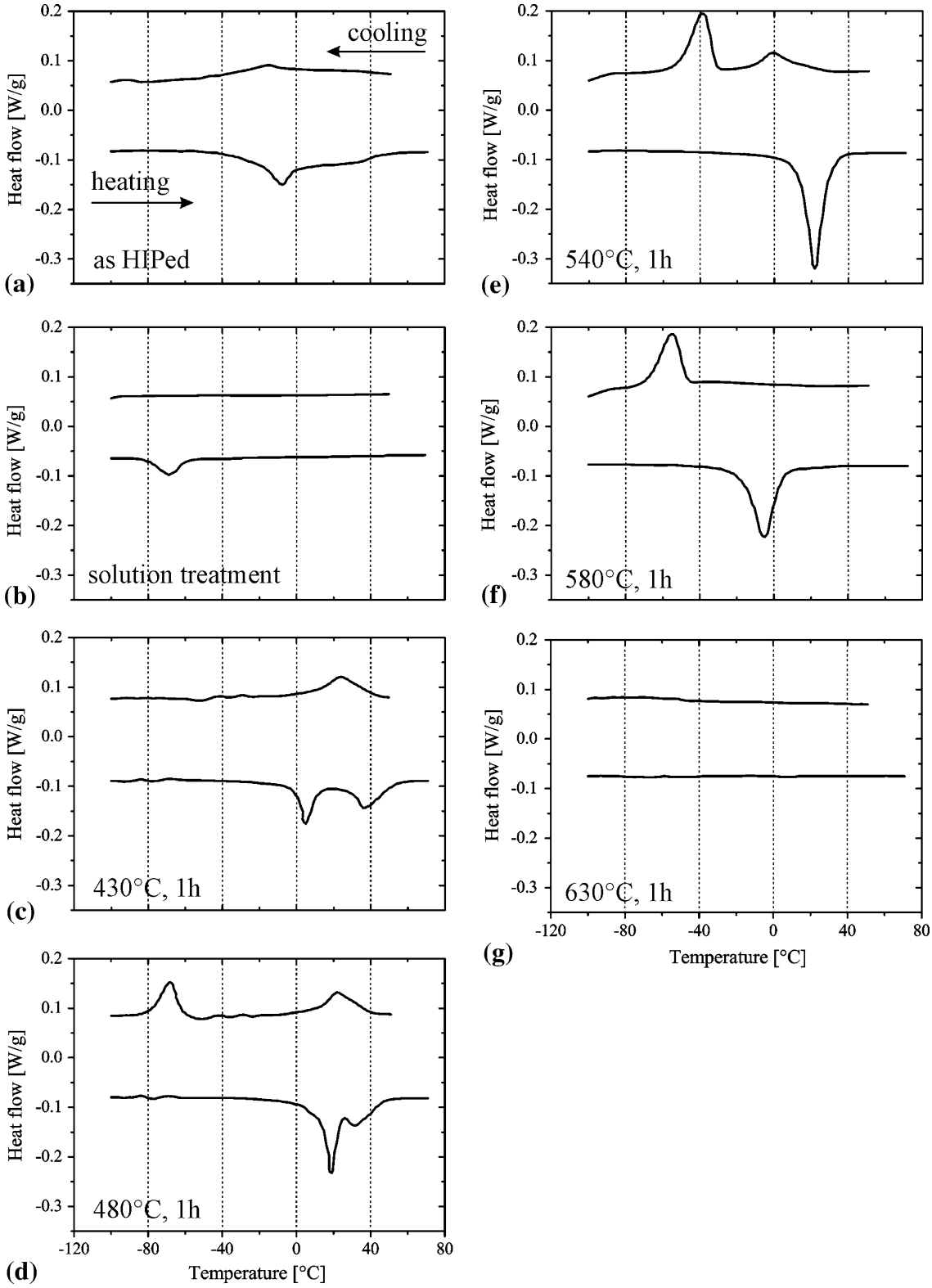

Fig. 6 Influence of annealing temperature on phase transformation temperatures of HIPed NiTi samples (Nan04, 1065 °C, 100 MPa, 3 h, solution treatment). (a) as HIPed, (b) solution treated at 1000 °C, 1 h and water quenched, annealing at (c) 430 °C, (d) 480 °C, (e) 540 °C, (f) 580 °C, and (g) 630 °C for 1 h (Ref 31)

60). For comparison, Kato et al. (Ref 21) and Johansen et al. (Ref 24) achieved similar stress-strain curves and plateau lengths for P/M NiTi made by HIP of prealloyed NiTi powders. Up to now, less information is given in the literature regarding the functional fatigue of P/M NiTi. In our work, it could be demonstrated that in the case of Ni-rich MIM samples, the repetition of thermal cycles (n = 9) did not change the phase transformation temperatures significantly within the accuracy of

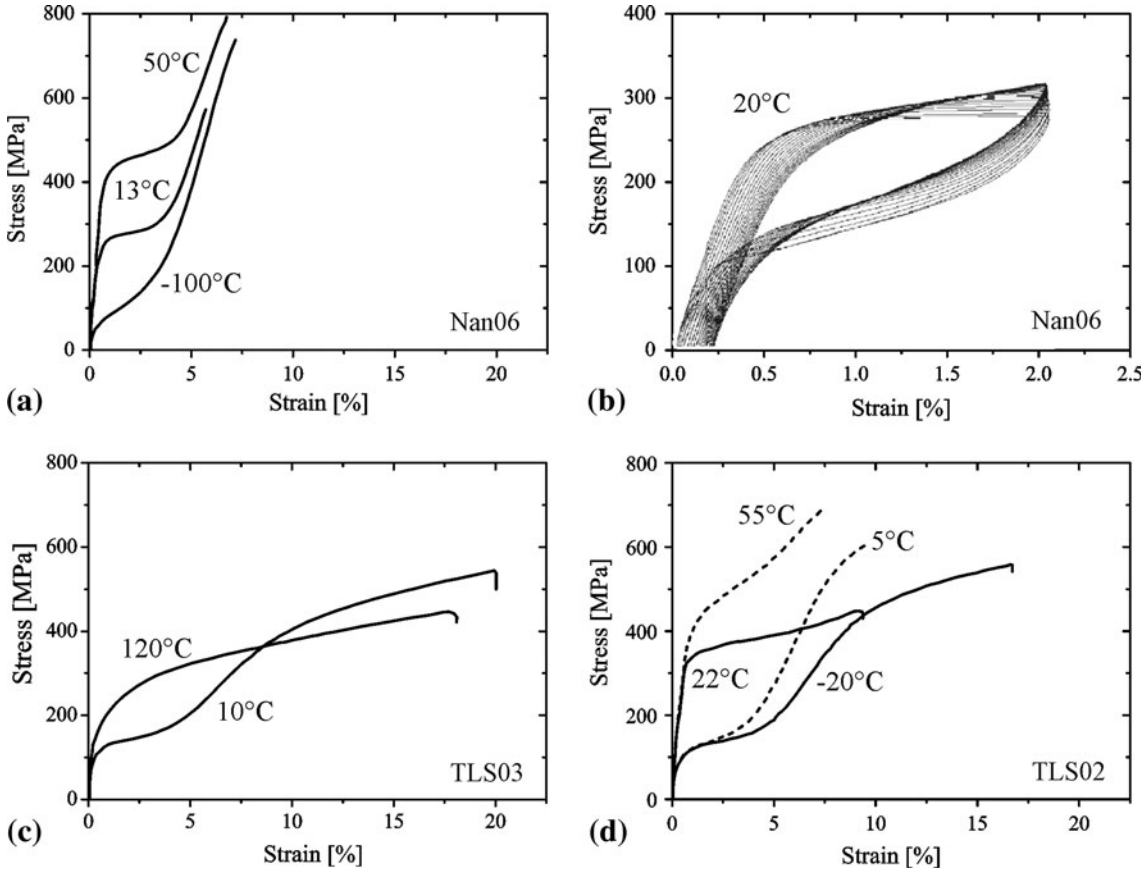

Fig. 7 Tensile tests on MIM samples sintered at 1250 °C, 5 h. (a) Tensile sample from powder fraction Nan06 as sintered without solution treatment, (b) fatigue of pseudoelasticity during first 20 load cycles (powder fraction Nan06) (Ref 29), (c) tensile sample from powder fraction TLS03, solution treated at 950 °C, 1 h, testing in the austenitic (120 °C) and martensitic (10 °C) state, (d) sample from powder fraction TLS02, solution treated at 950 °C, 1 h and annealed at 450 °C, 1 h (dotted lines) (Ref 32, 60)

the DSC equipment (Ref 29). The fatigue behavior during pseudoelastic cycles up to 2% deformation (Fig. 7b) was quite similar to that of NiTi prepared by ingot metallurgy (Ref 65). With increasing number of cycles, the critical stress for onset of stress-induced transformation decreased. This effect is accompanied by increase of the residual strain and decrease of mechanical hysteresis. In the case of P/M NiTi, a saturation of this behavior was observed after conducting more than 20 cycles (Ref 29). Changes in the microstructure as accumulation and reorientation of dislocations during phase transformation are proposed to be the main reason for fatigue of pseudoelasticity. For P/M NiTi, formation and movement of dislocations is significantly influenced by the increased amount of abovementioned lattice mismatch and precipitations.

3.6 Discussion of Factors Influencing Reproducibility of P/M NiTi

3.6.1 Availability of Prealloyed NiTi Powders. Up to now, full demonstration of reproducible P/M manufacturing of NiTi alloys starting from prealloyed NiTi powders is constrained by the fact that suitable starting powders, which were produced by comprehensive quality control regarding particle size distribution, impurity contents, and defined Ni:Ti ratio, were difficult to purchase on an industrial scale. Considering the results of our work, prealloyed NiTi powders produced by EIGA are more promising to achieve this aim, even if crop of particles smaller than 25 µm suitable for MIM processing is $<30\%$ so far. For making P/M of NiTi starting from these powders more economic, several P/M technologies were investigated in addition to MIM recently, aiming on the use of coarser NiTi powder fractions. In these applications, coarser NiTi powder fractions are even advantageous due to their improved flow ability and tapping density. HIP of encapsulated NiTi powders was used for the production of parts with low geometrical complexity like rings or tubes, which can be applied for coupling devices (Ref 66). Furthermore, NiTi tubes made by HIP may act as semi-finished parts for manufacturing of vascular stents, avoiding expensive manufacturing of thin-walled tubes by mechanical machining coupled with material loss. Even in the case of HIP, wall thickness must be further reduced by established hot or cold working followed by laser cutting of the filigree stent. Vacuum plasma spraying (VPS) has been demonstrated to be promising for deposition of wear-resistant coatings on parts, which are exposed to cavitation or erosion wear (Ref 67-69). In this case, pseudoelasticity of NiTi coating is discussed to cause significantly improved wear resistance. Last but not least, selective laser melting (SLM) or electron beam melting (EBM) of NiTi powder beds gains in importance within the last years enabling the net-shaped production of NiTi parts with complex geometries and optionally with regularly oriented macropores (Ref 70).

3.6.2 Residual Microporosity. Sintering of prealloyed NiTi powders is strongly influenced by low sintering activity of highly ordered, intermetallic NiTi phase (Ref 44, 45). Sintering

temperatures in the range of 1230-1265 °C, which is near the melting temperature of NiTi (1310 °C), and dwell times of at least 5 h are required to achieve sintering densities higher than 90% of theoretical density. Results of present work show that promising densities above 95% can be only achieved in the case of using Ni-rich NiTi alloys (e.g., with 50.8 at.% Ni) combined with particle sizes below 25 μm. If closed pores were achieved after sintering, post-compaction by HIP could be an effective measure to reduce residual porosity further. Sintering NiTi parts at abovementioned temperatures is coupled with the risk of chemical interaction between NiTi and sintering aid, which increases with temperature. Best results were achieved if an Y_2O_3 plate was used as sintering aid.

3.6.3 Uptake of Oxygen and Carbon During P/M Processing. P/M of NiTi alloys is strongly influenced by its high affinity to oxygen and carbon. Again, NiTi powders produced by EIGA process are most promising for keeping impurity contents at low level after P/M processing. Oxygen contents of EIGA powders were in the range of 0.09-0.10 wt.% for powder fractions smaller than 25 μm and in the range of 0.04-0.06 wt.% for intermediate powder fractions of 25-45 μm. In the case of HIP consolidation, oxygen content could be kept on the same level due to encapsulation of powders for load transfer. During MIM processing, further increase of oxygen content in the range of 0.05-0.10 wt.% is unavoidable due to contact with organic binder system and residual oxygen from sintering atmosphere. Sintering was preferentially done in vacuum with $p(O_2)$ below 10^{-3} Pa. By trend, smaller powder fractions lead to higher oxygen uptake. It must be mentioned that it was not possible to keep the oxygen content within the specification of ASTM-F2063-05, the standard norm of biomedical NiTi implants. On the other hand, uptake of carbon was found to be less critical. In the case of starting from EIGA powders, all P/M samples had carbon contents below 0.05 wt.%, therefore fulfilling ASTM-F2063-05. If application of MIM for net-shaped manufacturing of biomedical implants is aspired, critical discussion of accessible oxygen and carbon contents considering the particular requirement profile is needed.

It is well known that solubility of oxygen and carbon on interstitial sites of the NiTi lattice is almost negligible (Ref 50-53). Therefore, formation of oxygen-containing Ti_2Ni and TiC phases takes place. Since both phases are rich of Ti, shift of the Ni:Ti ratio of NiTi matrix to higher values results. This shift is coupled with lowering the phase transformation temperatures in the case that Ni content exceeds 50 at.%. Temperature shift can be calculated by well-known curve given by Tang et al. (Ref 37), Khalil-Allafi et al. (Ref 38), or Frenzel et al. (Ref 39). If prealloyed NiTi powders manufactured with comprehensive quality control are available, it is expected that shift of phase transformation temperatures due to formation Ti-rich secondary phases can be predicted with high accuracy.

3.6.4 Preliminary Attempt to Balance Ni:Ti Ratio. Recently, a promising attempt was conducted for adjusting phase transformation temperatures in the case of Ni-enrichment of NiTi matrix. It has been found that adding well-defined amount of elemental Ti powder to prealloyed NiTi powder might be suitable to balance the shift of Ni:Ti ratio caused by formation of abovementioned oxygen and carbon-containing secondary phases. Figure 8 shows a preliminary result demonstrating the feasibility of this idea.

3.6.5 Precipitation of Ni_4Ti_3 in the Case of Ni-Rich NiTi Alloys. Sintering of Ni-rich NiTi alloys is coupled with uncontrolled precipitation of Ni_4Ti_3, when slowly passing the temperature range of 630-350 °C during furnace cooling. For NiTi alloy with 50.8 at.% Ni cooled with 5 K/min, precipitation state was estimated from DSC measurements, which was correlated to anneal the same alloy in the temperature range of 400-450 °C for 1 h. It is well known from NiTi alloys made by ingot metallurgy that homogeneously distributed precipitation of meta-stable Ni_4Ti_3 is coupled with significant decrease of ductility (Ref 59). Therefore, it is advised to use P/M NiTi preferentially after solution treatment (e.g., 950 °C, 1 h) with subsequent water quenching, since residual microporosity and Ti-rich secondary phases are further sources for deterioration of mechanical properties compared to cast NiTi alloys.

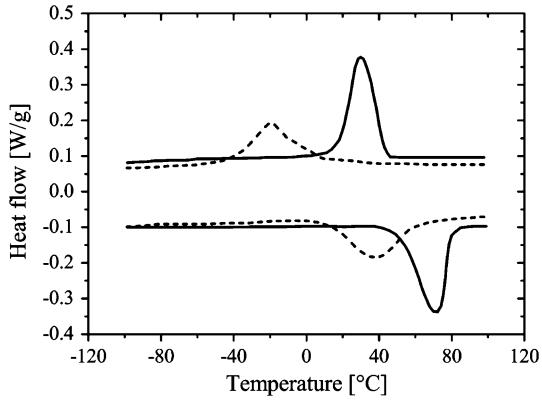

Fig. 8 MIM sample produced from TLS04 blended with 1 at.% Ti dealing for controlled adjustment of phase transformation temperatures by balancing Ni:Ti ratio of the matrix in the case of formation of Ti-rich secondary phases (dotted line: with 1 at.% Ti)

4. Summary

MIM of NiTi shape memory alloys starting from prealloyed NiTi powders is quite promising for net-shaped manufacturing of NiTi parts with fully pronounced shape memory effect or pseudoelasticity. Within the last decade, potential of this technology was already demonstrated on several prototypes including biomedical foot staple, tensile sample, and pipe connector sleeve. In the present work, a comprehensive study was conducted, which enabled to draw some general conclusions on P/M manufacturing of NiTi alloys. This study was based on experience achieved in our former work. Key factors influencing the reproducibility of P/M manufacturing of NiTi alloys are discussed in detail. The discussion includes the availability of prealloyed powders suitable for MIM processing, occurrence of residual porosity caused by low sintering activity of intermetallic NiTi phase, formation of Ti-rich secondary phases due to uptake of oxygen and carbon during P/M processing as well as precipitation of meta-stable Ni_4Ti_3 phases, which might already occur during cooling from sintering temperature. Last but not least, influence of these key factors on shape memory and mechanical properties is discussed in detail.

Acknowledgments

The authors thank the Deutsche Forschungsgemeinschaft DFG for financially supporting this work within the framework of SFB459 (Shape Memory Technology) in the period of 1999-2011. The

contributions of Dr. Juliane Mentz as well as of the former PhD students Dr. Lars Krone and Dr. Manuel Köhl are highly acknowledged.

References

1. M. Igharo and J.V. Wood, Compaction and Sintering Phenomena in Titanium-Nickel Shape Memory Alloys, *Powder Metall.*, 1985, **28**, p 131–139
2. H.C. Yi and J.J. Moore, The Combustion Synthesis of Ni-Ti Shape Memory Alloys, *J. Mater.*, 1990, **42**, p 31–35
3. M. Zhu, T.C. Li, J.T. Liu, and D.Z. Yang, Microstructure Characteristics of NiTi Shape Memory Alloy Obtained by Explosive Compact of Elemental Nickel and Titanium Powders, *Acta Metall. Mater.*, 1991, **39**, p 1481–1487
4. J.C. Hey and A.P. Jardine, Shape Memory TiNi Synthesis from Elemental Powders, *Mater. Sci. Eng. A*, 1994, **188**, p 291–300
5. B.Y. Li, L.J. Rong, Y.Y. Li, and V.E. Gjunter, Synthesis of Porous Ni-Ti-Shape-Memory Alloys by Self-Propagating Synthesis: Reaction Mechanism and Anisotropy in Pore Structure, *Acta Mater.*, 2000, **48**, p 3895–3904
6. B. Bertheville and J.E. Bidaux, Alternative Powder Metallurgical Processing of Ti-Rich NiTi Shape Memory Alloys, *Scripta Mater.*, 2005, **52**, p 507–512
7. B.Y. Li, L.J. Rong, and Y.Y. Li, The Influence of Addition of TiH_2 in Elemental Powder Sintering Porous Ni-Ti Alloys, *Mater. Sci. Eng. A*, 2000, **281**, p 169–175
8. D.C. Lagoudas and E.L. Vandygriff, Processing and Characterization of NiTi Porous SMA by Elevated Pressure Sintering, *J. Intell. Mater. Syst. Struct.*, 2002, **13**, p 837–850
9. Y.P. Zhang, B. Yuan, M.Q. Zeng, C.Y. Chung, and X.P. Zhang, High Porosity and Large Pore Size Shape Memory Alloys Fabricated by Using Pore-Forming Agent (NH_4HCO_3) and Capsule-Free Hot Isostatic Pressing, *J. Mater. Process. Technol.*, 2007, **192**, p 434–442
10. D.S. Li, Y.P. Zhang, G. Eggeler, and X.P. Zhang, High Porosity and High Strength Porous NiTi Shape Memory Alloy with Controllable Pore Characteristics, *J. Alloys Compd. Lett.*, 2009, **470**, p L1–L5
11. C.L. Chu, C.Y. Chung, and P.H. Lin, Influence of Solution Treatment on the Compressive Properties of Porous NiTi Shape Memory Alloy of 53.4 vol.% Ni Fabricated by Combustion Synthesis, *J. Mater. Sci. Lett.*, 2004, **39**, p 4949–4951
12. M. Bram, A. Ahmad-Khanlou, A. Heckmann, B. Fuchs, H.P. Buchkremer, and D. Stöver, Powder Metallurgical Fabrication Processes for NiTi Shape Memory Alloys, *Mater. Sci. Eng. A*, 2002, **337**, p 254–263
13. B. Yuan, C.Y. Chung, and M. Zhu, Microstructure and Martensitic Transformation Behavior of Porous NiTi Shape Memory Alloy Prepared by Hot Isostatic Pressing Processing, *Mater. Sci. Eng., A*, 2004, **382**, p 181–187
14. S.L. Zhu, X.J. Yang, F. Hu, S.H. Deng, and Z.D. Cui, Processing of Porous TiNi Shape Memory Alloy from Elemental Powders by Ar-Sintering, *Mater. Lett.*, 2004, **58**, p 2369–2373
15. T.B. Massalski, H. Okamato, P.R. Subramanian, and L. Kacprzak, Ed., *Binary Alloy Phase Diagrams*, 2nd ed., ASM International, Materials Park, OH, 1996
16. M. Assad, P. Jarzem, M.A. Leroux, C. Coillard, A.V. Chernyshov, and S. Charette, Porous Titanium-Nickel for Intervertebral Fusion in a Sheep Model, Part 1: Histophometric and Radiological Analysis 1, *J. Biomed. Mater. Res. B*, 2003, **B64**, p 107–120
17. S. Rhalmi, S. Charette, M. Assad, C. Coillard, and C.H. Rivard, The Spinal Cord Dura Mater Reaction to Nitinol and Titanium Alloy Particles: A 1-Year Study in Rabbits, *Eur. Spine J.*, 2007, **16**, p 145–154
18. W.A. Johnson, J.A. Domingue, and S.A. Reichman, P/M Processing and Characterization of Controlled Transformation Temperature of NiTi, *J. Phys. Colloq.*, 1982, **C4**(43), p 285–290
19. M. Igharo and J.V. Wood, Consolidation of Rapidly Solidified Ti-Ni Intermetallics, *Powder Metall.*, 1986, **29**, p 37–41
20. H. Kato, T. Koyari, S. Miura, K. Isonishi, and M. Tokinaze, Shape Memory Characteristics in Powder Metallurgy TiNi Alloys, *Scripta Met. Mater.*, 1990, **24**, p 2335–2340
21. H. Kato, T. Koyari, M. Tokazane, and S. Miura, Stress Strain Behavior and Shape Memory Effect in Powder Metallurgy TiNi Alloys, *Acta Metall. Mater.*, 1994, **42**, p 1351–1358
22. T.W. Duerig, Ni-Ti Shape Memory Alloys by Powder Metallurgical Methods, *Proc. of First Int. Conf. on Shape Memory and Superelastic Technologies SMST94*, A.R. Pelton, Ed., ASM The Materials Information Society, Pacific Grove, California, USA, 1994, p 31–42
23. D. Mari and D.C. Dunand, NiTi and NiTi-TiC Composites: Part 1: Transformation and Thermal Cycling Behavior, *Met. Mater. Trans. A*, 1995, **26**, p 2823–2847
24. K. Johansen, H. Voggenreiter, and G. Eggeler, On the Effect of TiC Particles on the Tensile Properties and on the Intrinsic Two Way Effect of NiTi Shape Memory Alloys Produced by Powder Metallurgy, *Mater. Sci. Eng., A*, 1999, **273–275**, p 410–414
25. Y.Y. Zhao, T. Fung, L.P. Zhang, and F.L. Zhang, Lost Carbonate Sintering Process for Manufacturing Metal Foams, *Scripta Mater.*, 2005, **52**, p 295–298
26. P. Imgrund, A. Rota, H. Schmidt, and G. Capretti, μ-MIM: Making the Most of NiTi, *Met. Powder Rep.*, 2008, **63**, p 21–24
27. L. Krone, E. Schüller, M. Bram, O.A. Hamed, H.P. Buchkremer, and D. Stöver, Mechanical Behaviour of NiTi Parts Prepared by Powder Metallurgical Methods, *Mater. Sci. Eng., A*, 2004, **378**, p 185–190
28. L. Krone, Metal Injection Moulding (MIM) von NiTi Bauteilen mit Formgedächtnis-Eigenschaften, PhD Thesis, Ruhr-Universität Bochum, 2005
29. L. Krone, J. Mentz, M. Bram, H.P. Buchkremer, D. Stöver, M. Wagner, G. Eggeler, D. Christ, S. Reese, D. Bogdanski, M. Köller, S.A. Esenwein, G. Muhr, O. Prymak, and M. Epple, The Potential of Powder Metallurgy for the Fabrication of Biomaterials on the Basis of Nickel-Titanium: A Case Study with a Staple Showing Shape Memory Behaviour, *Adv. Eng. Mater.*, 2005, **7**, p 613–619
30. J. Mentz, M. Bram, H.P. Buchkremer, and D. Stöver, Improvement of Mechanical Properties of Powder Metallurgical NiTi Shape Memory Alloys, *Adv. Eng. Mater.*, 2006, **8**, p 247–252
31. J. Mentz, L. Krone, M. Bram, H.P. Buchkremer, and D. Stöver, Influence of Heat Treatment on Properties of Hot Isostatic Pressed (HIP) NiTi, *Int. Conf. on Shape Memory and Superelastic Technologies, SMST*, 3–7 October 2004, Baden-Baden, Germany, 2006, p 489–494
32. J. Mentz, M. Bram, H.P. Buchkremer, and D. Stöver, Influence of Heat Treatments on the Mechanical Properties of High-Quality Ni-Rich NiTi Produced by Powder Metallurgical Methods, *Mater. Sci. Eng., A*, 2008, **481–482**, p 630–634
33. J. Mentz, J. Frenzel, M.F.X. Wagner, K. Neuking, G. Eggeler, H.P. Buchkremer, and D. Stöver, Powder Metallurgical Processing of NiTi Shape Memory Alloys with Elevated Transformation Temperatures, *Mater. Sci. Eng., A*, 2008, **491**, p 270–278
34. M. Köhl, T. Habijan, M. Bram, H.P. Buchkremer, D. Stöver, and M. Köller, Powder Metallurgical Near-Net-Shape Fabrication of Porous NiTi Shape Memory Alloys for Use as Long Term Implants by the Combination of the Metal Injection Moulding Process with the Space Holder Technique, *Adv. Eng. Mater.*, 2009, **11**, p 959–968
35. M. Köhl, M. Bram, A. Moser, T. Beck, H.P. Buchkremer, and D. Stöver, Characterization of Porous, Net-Shaped Ti and NiTi Alloys Regarding Their Damping and Energy Absorbing Capacity, *Mater. Sci. Eng., A*, 2011, **528**, p 2452–2462
36. M. Bram, M. Köhl, H.P. Buchkremer, and D. Stöver, Mechanical Properties of Highly Porous NiTi Alloys, *J. Mater. Eng. Perform.*, 2011, **20**, p 522–528
37. W. Tang, B. Sundmann, R. Sandström, and C. Quiu, New Modelling of the B2 Phase and its Associated Martensitic Transformation in the Ti-Ni System, *Acta Mater.*, 1999, **47**, p 3457–3468
38. J. Khalil-Allafi, A. Dlouhy, and G. Eggeler, Ni_4Ti_3-Precipitation During Aging of NiTi Shape Memory Alloys and its Influence on Martensitic Phase Transformations, *Acta Mater.*, 2002, **50**, p 4255–4274
39. J. Frenzel, E.P. George, A. Dlouhy, C. Somsen, M.X.F. Wagner, and G. Eggeler, Influence of Ni on Martensitic Transformations in NiTi Shape Memory Alloys, *Acta Mater.*, 2010, **58**, p 3444–3458
40. L. Gerking, Powder from Metal and Ceramic Melts by Laminar Gas Stream at Supersonic Speeds, *Powder Met. Int.*, 1993, **25**, p 59–65
41. W. Schatt, K.P. Wieters, and B. Kieback, *Pulvermetallurgie—Technologie und Werkstoffe*, Springer, Berlin, Heidelberg, New York, 2007
42. A. Bansiddhi and D.C. Dunand, Shape-Memory NiTi Foams Produced by Solid State Replication with NaF, *Intermetallics*, 2007, **15**, p 1612–1622
43. M. Nishida, C.M. Wayman, and T. Honma, Precipitation Process in Near-Equiatomic TiNi Shape Memory Alloys, *Metall. Trans. A*, 1986, **17**, p 1505–1515

44. G.F. Bastin and G.D. Rieck, Diffusion in the Titanium-Nickel System: I. Occurrence and Growth of Various Intermetallic Compounds, *Metall. Trans.*, 1997, **5**, p 1817–1826
45. H. Mehrer, Diffusion in Binary Intermetallics, *Diffusion in Solids: Fundamentals, Methods, Materials, Diffusion-Controlled Processes*, H. Mehrer, Ed., Springer, Berlin, Heidelberg, 2007, p 341–369
46. Lexikon der Physik, CD-Rom, Spektrum Akademischer Verlag, Heidelberg, 2000
47. M. Köhl, Endkonturnahe Herstellung von biomedizinischen Implantaten mit definierter Porosität durch Metallpulverspritzgießen, PhD thesis, Ruhr-Universität Bochum, 2009
48. J.L. Murray and H.A. Wriedt, The O-Ti (Oxygen-Titanium) System, *Bull. Alloy Phase Diagr.*, 1987, **8**, p 148–165
49. H. Okamoto, Comment on C-Ti (Carbon-Titanium), *J. Phase Equilib.*, 1995, **16**, p 522–523
50. E.R. Stover and J. Wulff, The Nickel-Titanium-Carbon System, *Trans. AIME*, 1959, **215**, p 127–136
51. Y. Shugo, S. Hanada, and T. Honma, Effect of Oxygen Content on the Martensite Transformation and Determination of Defect Structure in TiNi alloys, *Bull. Res. Inst. Miner. Dress. Metall.*, 1985, **41**, p 23–34
52. T. Saburi, TiNi Shape Memory Alloys, *Shape Memory Materials*, K. Otsuka and C.M. Wayman, Ed., Cambridge University Press, Cambridge, 1998
53. T.W. Duerig, A.R. Pelton, and C. Trepanier, Nitinol, Chapter 9: Alloying and Composition, *SMST e-Elastic Newsletter*, www.asminternational.org, 2011
54. C.M. Jackson, H.J. Wagner, and R.J. Wasilesky, 55-Nitinol—The Alloy with a Memory: Its Physical Metallurgy, Properties and Applications, NASA publication SP-5110, Washington, DC, USA, 1972, p 42–59
55. P. Olier, F. Barcelo, J.L. Bechade, J.C. Brachet, E. Lefevre, and G. Guenin, Effects of Impurities Content (Oxygen, Carbon, Nitrogen) on Microstructure and Phase Transformation Temperatures of Near Equiatomic TiNi Shape Memory Alloys, *J. Phys. IV*, 1997, **7**, p 143–148
56. K. Otsuka and X. Ren, Physical Metallurgy of Ti-Ni-Based Shape Memory Alloys, *Prog. Mater. Sci.*, 2005, **50**, p 511–678
57. T. Tadaki, Y. Nakata, K. Shimizu, and K. Otsuka, Crystal Structure, Composition and Morphology of a Precipitate in an Aged Ti-51 at% Ni Shape Memory Alloy, *Trans. Jpn. Inst. Met.*, 1986, **27**, p 731–740
58. K. Otsuka and M.C. Wayman, *Shape Memory Materials*, Cambridge University Press, Cambridge, 1998
59. S. Miyazaki, Y. Kohiyama, K. Otsuka, and T.W. Duerig, Effects of Several Factors on the Ductility of the Ti-Ni Alloy, *Mater. Sci. Forum*, 1990, **56–58**, p 765–770
60. J. Mentz, M. Bram, H.P. Buchkremer, and D. Stöver, Improvement of Mechanical Properties of Powder Metallurgical NiTi by Reduction of Impurity Phases, *Int. Conf. on Shape Memory and Superelastic Technologies SMST*, 7–11 May 2006, B. Berg, M.R. Mitchell, J. Proft, Ed., Pacific Grove, California, USA, 2008, p 399–408
61. T. Saburi, M. Yoshida, and S. Nenno, Deformation Behavior of Shape Memory Ti-Ni Alloy Crystals, *Scripta Metall.*, 1984, **18**, p 363–366
62. S. Miyazaki, S. Kimura, K. Otsuka, and Y. Suzuki, The Habit Plane and Transformation Strain with the Martensitic Transformation in TiNi Single Crystals, *Scripta Metall.*, 1984, **18**, p 883–890
63. Y. Liu, Z. Xie, J. van Humbeeck, and L. Delaey, Asymmetry of Stress-Strain Curves Under Tension and Compression for NiTi Shape Memory Alloys, *Acta Mater.*, 1998, **46**, p 4325–4338
64. D.E. Hodgson and J.W. Brown, *Using Nitinol Alloys*, Shape Memory Applications Inc., San Jose, CA, 2000
65. G. Eggeler, E. Hornbogen, A. Yawny, A. Heckmann, and M. Wagner, Structural and Functional Fatigue of NiTi Shape Memory Alloys, *Mater. Sci. Eng., A*, 2004, **378**, p 24–33
66. M. Köhl, M. Bram, B. Coenen, H.P. Buchkremer, and D. Stöver, Herstellung von Halbzeugen aus NiTi-Legierungen, German Patent DE 10 2007 047 523, 2007
67. M. Bram, A. Ahmad-Khanlou, H.P. Buchkremer, and D. Stöver, Vacuum Plasma Spraying of NiTi Protection Layers, *Mater. Lett.*, 2002, **57**, p 647–651
68. J. Stella, E. Schüller, C. Heßing, O.A. Hamed, M. Pohl, and D. Stöver, Cavitation Erosion of Plasma-Sprayed NiTi Coatings, *Wear*, 2006, **260**, p 1020–1027
69. G. Mauer, R. Vaßen, and D. Stöver, Controlling the Oxygen Contents in Vacuum Plasma Sprayed Metal Alloy Coatings, *Surf. Coat. Technol.*, 2007, **201**, p 4796–4799
70. H. Meier, C. Haberland, J. Frenzel, and R. Zarnetta, Selective Laser Melting of NiTi Shape Memory Alloys, *Innovative Developments in Design and Manufacturing—Advanced Research in Virtual and Rapid Prototyping*, 2010, p 233–238